

SCIENTIFIC REPORTS

OPEN

Photocatalytic generation of hydrogen by core-shell $\text{WO}_3/\text{BiVO}_4$ nanorods with ultimate water splitting efficiency

Received: 02 February 2015

Accepted: 11 May 2015

Published: 08 June 2015

Yuriy Pihosh^{1,*}, Ivan Turkevych^{2,4,*}, Kazuma Mawatari¹, Jin Uemura¹, Yutaka Kazoe¹, Sonya Kosar^{1,3}, Kikuo Makita², Takeyoshi Sugaya², Takuya Matsui², Daisuke Fujita⁴, Masahiro Tosa⁴, Michio Kondo² & Takehiko Kitamori¹

Efficient photocatalytic water splitting requires effective generation, separation and transfer of photo-induced charge carriers that can hardly be achieved simultaneously in a single material. Here we show that the effectiveness of each process can be separately maximized in a nanostructured heterojunction with extremely thin absorber layer. We demonstrate this concept on $\text{WO}_3/\text{BiVO}_4+\text{CoPi}$ core-shell nanostructured photoanode that achieves near theoretical water splitting efficiency. BiVO_4 is characterized by a high recombination rate of photogenerated carriers that have much shorter diffusion length than the thickness required for sufficient light absorption. This issue can be resolved by the combination of BiVO_4 with more conductive WO_3 nanorods in a form of core-shell heterojunction, where the BiVO_4 absorber layer is thinner than the carrier diffusion length while its optical thickness is reestablished by light trapping in high aspect ratio nanostructures. Our photoanode demonstrates ultimate water splitting photocurrent of 6.72 mA cm^{-2} under 1 sun illumination at $1.23 \text{ V}_{\text{RHE}}$ that corresponds to ~90% of the theoretically possible value for BiVO_4 . We also demonstrate a self-biased operation of the photoanode in tandem with a double-junction $\text{GaAs}/\text{InGaAsP}$ photovoltaic cell with stable water splitting photocurrent of 6.56 mA cm^{-2} that corresponds to the solar to hydrogen generation efficiency of 8.1%.

Bismuth vanadate (BiVO_4) is one of the most promising materials for the photocatalytic production of hydrogen¹ via water splitting with a relatively narrow bandgap of 2.4 eV in the monoclinic phase, excellent stability against photocorrosion and low cost. Theoretical solar to hydrogen (STH) efficiency of BiVO_4 approaches 9.2% with the photocurrent of 7.5 mA cm^{-2} under the standard AM1.5G solar light illumination. Despite being a good absorber with a direct bandgap, BiVO_4 has poor electron transport properties² due to a high recombination rate of photogenerated carriers. As a result, BiVO_4 is characterized by a short carrier diffusion length (L_d) of around 70 nm³, which is the main reason why the first generation of BiVO_4 photoanodes demonstrated small photocurrents of less than 1 mA cm^{-2} at $1.23 \text{ V}_{\text{RHE}}$ ⁴⁻⁹.

In addition to poor electron transport properties, slow transfer of holes at the $\text{BiVO}_4/\text{electrolyte}$ interface is another performance limiting factor. Coupling of BiVO_4 with RhO_2 ¹⁰, cobalt-phosphate

¹Department of Applied Chemistry, School of Engineering, The University of Tokyo, 7-3-1 Hongo, Bunkyo, Tokyo 113-8656, Japan. ²National Institute of Advanced Industrial Science and Technology (AIST), AIST Central 2-13, Tsukuba, Ibaraki 305-0047, Japan. ³Chernivtsy National University, Institute of Physics, Engineering and Computer Science, Storozhynetska 101, Chernivtsy, 58000 Ukraine. ⁴National Institute for Materials Science (NIMS), 1-2-1 Sengen, Tsukuba, Ibaraki 305-0047, Japan. *These authors contributed equally to this work. Correspondence and requests for materials should be addressed to Y.P. (email: pihosh@icl.t.u-tokyo.ac.jp) or T.K. (email: kitamori@icl.t.u-tokyo.ac.jp)

(CoPi)^{11–14} or FeOOH/NiOOH¹⁵ co-catalysts helped to improve the kinetics of oxygen evolution reaction (OER) significantly. Since the development of efficient OER co-catalysts, the bulk electronic conductivity was identified as a remaining performance bottleneck of BiVO₄ photoanodes³. Although the attempts to enhance transport properties of BiVO₄ by doping with Mo¹⁴ or W^{12,13} quickly raised photocurrent to 2.3 mA cm⁻²¹⁶, and then to 3.6 mA cm⁻²¹⁷, at 1.23 V_{RHE} by using a gradual doping profile and CoPi OER co-catalyst, these photocurrents were still smaller than 50% of the theoretically possible value of 7.5 mA cm⁻². The combination of BiVO₄ with more conductive WO₃ in a form of a planar heterojunction resulted in similar photocurrents of 2.8 mA cm⁻² for simple WO₃/BiVO₄ and 3.04 mA cm⁻² for a WO₃/SnO₂/BiVO₄ structure with a SnO₂ blocking layer. The type II band alignment at the heterojunction interface helped to improve separation of the photogenerated carriers. However, the photocurrent remained limited, because the L_d was still shorter than the thickness of the BiVO₄ film, that was required to gain a sufficient light absorption.

An alternative approach to compensate for the short L_d is to use an extremely thin absorber (ETA) heterojunction structure, where the BiVO₄ absorber is thinner than the L_d while the optical thickness is reestablished by a structured interface with a high aspect ratio. The ETA structure significantly improves collection probability of photogenerated carriers, because they do not need to travel over large distances before separation. Another important advantage of the ETA structure is the efficient light scattering that increases the optical path through the device and thereby enhances the photon absorption. As a result, photocurrent in the photoanode can be maximized by separate optimization of optical and electronic thicknesses of the BiVO₄ absorber.

The first WO₃/BiVO₄ heterojunction photoanode with a nanostructured interface was demonstrated by Su *et al.*¹⁸ Their photoanode was based on disordered WO₃ nanowires (NW) prepared by a solvothermal method without formation of a fully developed ETA structure. As a result, the photocurrent was limited to less than 1 mA cm⁻². Further progress was focused on preparation of fully developed and uniform 1D core-shell WO₃/BiVO₄ structures. Although the ETA photoanodes based on chemically prepared WO₃-NWs demonstrated improved photocurrents of 2.4 mA cm⁻² by Pilli *et al.*¹⁹ and 3.1 mA cm⁻² by Rao *et al.*²⁰, it was clear that the structurally defective WO₃-NWs are responsible for high resistive losses in the structure. Thus, preparation of sufficiently conductive, uniform and vertically standing WO₃ nanostructures with a high aspect ratio appeared as a key factor for realization of efficient WO₃/BiVO₄ heterojunction photoanodes.

In our previous work²¹ we firstly demonstrated a WO₃/BiVO₄ heterojunction photoanode based on WO₃ nanorods (NRs) fabricated by Glancing Angle Deposition (GLAD). After application of the CoPi OER co-catalyst we achieved the photocurrent of 3.2 mA cm⁻² at 1.23 V_{RHE}, that was the record photocurrent among published for BiVO₄ photoanodes at that time. We demonstrated that the WO₃-NRs prepared by GLAD provide highly efficient pathways for photogenerated electrons and outlined that further optimization of the WO₃-NRs/BiVO₄ core-shell structure toward better conformality of the BiVO₄ ETA layer should lead to a nearly theoretical photocurrent. Here we report the optimized WO₃-NRs/BiVO₄+CoPi photoanode with the record photocurrent of 6.72 mA cm⁻² at 1.23 V_{RHE} that approaches 90% of the theoretically possible value. To the best of our knowledge, this is the highest photocurrent reported up to date for a water splitting photoanode.

During preparation of this manuscript Shi *et al.*²² reported a WO₃-NRs/BiVO₄:W,Mo-doped photoanode based on helical WO₃-NRs deposited by GLAD. Their photoanode demonstrated the photocurrent of 4.2 mA cm⁻² with CoPi and 5.35 mA cm⁻² with FeOOH/NiOOH co-catalysts. Although their helical nanostructure showed complete absorption of the incident light, the absorption edge of the Mo,W-doped BiVO₄ was blue-shifted due to doping. Also, the thickness of the BiVO₄ layer in their nanostructure was rather small, that in turn required very long helical WO₃ nanorods of 5.5 μm to gain the optical thickness. As a result, the combined effect of the blue shift and resistive losses in the long WO₃ nanorods limited the photocurrent of their device to 5.35 mA cm⁻², which is near 70% of the possible theoretical value. Also, Shi *et al.* attributed the performance enhancement to the helical morphology of their WO₃-NRs. However, they did not compare the performance of helical and plain nanorods experimentally. Their conclusion about significant contribution of the helical morphology to the light trapping relies on the finite element frequency domain (FEFD) simulations of WO₃-NRs without including the BiVO₄ ETA layer into the model. From a ray-optics perspective, the absorption enhancement factor due to light trapping at rough interfaces is given by $4n^2$, where n is the refractive index of the absorber²³. Since the refractive indexes of WO₃ and BiVO₄ are both close to 2.5^{24,25}, we can expect sufficient light trapping even in case of plain nanorod morphology. Indeed, in this work we achieved 20% higher photocurrent than Shi *et al.* by using plain WO₃-NRs of a much shorter length of only 2.5 μm and an undoped BiVO₄+CoPi absorber layer with an optimized thickness of around 25 nm.

We also examined the combined influence of light intensity and temperature on the performance of our photoanode. Photocatalytic water splitting is a chemical reaction and thus will accelerate with increase of temperature according to the Arrhenius relation. Therefore, previously unused infrared light can heat the cell and contribute to water splitting by improving the reaction kinetics. It turns out that this feature is of special importance for the efficient performance of PEC under concentrated light, as it helps to significantly reduce recombination losses due to improved charge transfer kinetics at a photoanode/electrolyte interface and thus to avoid the typical sub-linear dependence of photocurrent on light

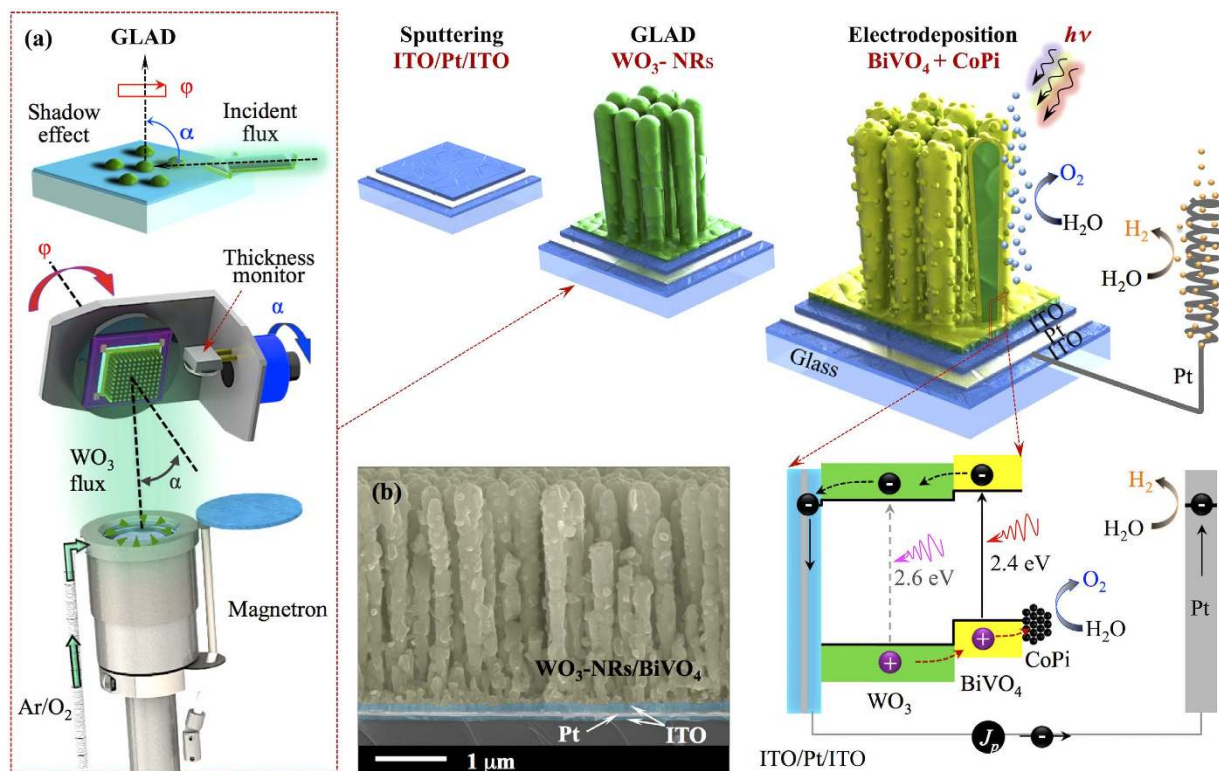


Figure 1. Schematic illustration of a core-shell $\text{WO}_3\text{-NRs/BiVO}_4$ photoanode fabricated by glancing angle deposition (GLAD) of $\text{WO}_3\text{-NRs}$ followed by electrodeposition of $\text{BiVO}_4\text{+CoPi}$. The inset (a) illustrates GLAD. The SEM image (b) shows a cross section of the $\text{ITO/Pt/ITO/WO}_3\text{-NRs/BiVO}_4\text{+CoPi}$ photoanode.

intensity²⁶. In this work we demonstrate that our photoanode achieves a stable photocurrent of 18.2 mA cm^{-2} under concentrated light of 3 suns at the cell temperature of 50°C .

Spontaneous water splitting requires a photocatalytic material with conduction and valence bands positions that provide sufficient overpotentials for H_2 and O_2 evolution half-reactions. Unfortunately, the position of the BiVO_4 conduction band does not fulfil that condition, and the photoanode needs an additional bias potential to drive the H_2 evolution half-reaction. Construction of a photoanode/photovoltaic tandem is a good approach to fabricating a self-biased water splitting cell. Previously, mechanically stacked tandems, based on a dye-sensitized solar cell (DSSC) with Fe_2O_3 or WO_3 photoanodes²⁷, and monolithic tandems, based on single- or double-junction a-Si solar cells with $\text{BiVO}_4\text{:Mo+CoPi}$ photoanode layers¹⁷, demonstrated self-biased photocurrents of 1.34, 2.23, 3.0 and 4.0 mA cm^{-2} , respectively. In all the cases the performance was affected by inferior transparency of the top BiVO_4 photoanode. Since our photoanode can efficiently operate under concentrated light, which saves a lot of lateral space, we can accommodate alternative tandem configurations. Here we demonstrate a PEC-PV tandem device based on a $\text{WO}_3\text{-NRs/BiVO}_4\text{+CoPi}$ photoanode biased by a GaAs/InGaAsP solar cell that operates under reflected light from the photoanode. The PEC-PV tandem achieves a stable water splitting photocurrent of 6.56 mA cm^{-2} at standard conditions and 18.17 mA cm^{-2} at 3 suns and elevated cell temperature of 50°C .

Results and Discussion

We fabricated the photoanode by a combination of GLAD of $\text{WO}_3\text{-NRs}$ and subsequent Electrochemical Deposition (ED) of BiVO_4 and CoPi (Fig.1). The details of the fabrication process can be found in experimental section. Scanning electron microscopy (SEM) studies of the optimized $\text{WO}_3\text{-NRs}$ and $\text{WO}_3\text{-NRs/BiVO}_4$ reveals that the nanorods are well separated and uniform with the length of $2.5\mu\text{m}$ and the average diameter varying from 200 to 300 nm along the nanorods (Supplementary Fig. S1). This length was selected as optimal based on our previous work²¹. In order to optimize the thickness of the electrodeposited BiVO_4 layer we studied the dependence of the photocurrent of $\text{WO}_3\text{-NRs/BiVO}_4$ samples measured at $1.23\text{ V}_{\text{RHE}}$ under the standard AM1.5G illumination on the total charge density that passed during the electrodeposition of BiVO_4 . The total charge density is proportional to the quantity of the deposited BiVO_4 and thus to the average thickness of the BiVO_4 layer. The increase of the BiVO_4 layer thickness boosts light absorption and thus the photocurrent. When the thickness of the BiVO_4 becomes

comparable with the L_d , the bulk recombination starts to prevail and the photocurrent decreases. The SEM observation of the samples reveals that the electrodeposition starts from the conformal growth of the BiVO_4 layer and then proceeds with formation of hemispherical clusters. Finally, the overgrown clusters fill the gaps between the nanorods (Supplementary Fig. S2). The Scanning Probe Microscopy (SPM) studies of the topography and local current maps of WO_3 -NRs and WO_3 -NRs/ BiVO_4 samples indicate that the WO_3 -NRs are coated by a conformal BiVO_4 layer with hemispherical clusters, that corresponds to the “layer-plus-island” Stranski–Krastanov growth mode during the electrodeposition (Supplementary Fig. S3). Also, the elemental distributions of W, Bi and V measured across a single WO_3 nanorod with a BiVO_4 layer by energy dispersive X-ray spectroscopy confirms its core-shell structure with Bi and V maxima near the edge of the nanorod (Supplementary Fig. S4). The monoclinic phases for WO_3 ²⁸ nanorods with triplet peaks at 23.0° (002), 23.5° (020) and 24.3° (200) and BiVO_4 ²⁹ with characteristic peaks at 18.9° (110), 29.2° (112) and 31.0° (200) were confirmed by XRD analysis (Supplementary Fig. S5).

The subsequent photo-assisted electrodeposition of a CoPi OER co-catalyst elevated the photocurrent density from 5.45 mA cm^{-2} to 6.72 mA cm^{-2} at $1.23 \text{ V}_{\text{RHE}}$ for the optimized sample (Supplementary Fig. S2a). Figure S6 shows I-V characteristics of optimized WO_3 -NRs, WO_3 -NRs/ BiVO_4 and WO_3 -NRs/ BiVO_4 +CoPi photoanodes measured in a three-electrode configuration under standard conditions. According to the commonly accepted PEC characterization protocol³⁰, developed to standardize evaluation of water splitting PEC devices, the photoanode performance has to be characterized in a two-electrode configuration, because application of a potential bias versus a reference electrode excludes the second half-reaction at a counter electrode. For that reason, we performed further PEC characterizations in the two-electrode configuration with a Pt counter electrode. After comparing the I-V characteristics of the same photoanode measured in two- and three-electrode configurations, we estimated that the same photocurrent of 6.72 mA cm^{-2} measured at $1.23 \text{ V}_{\text{RHE}}$ in the three-electrode configuration is achieved at the bias of 1.02 V in the two-electrode configuration (Supplementary Fig. S7). Since the onset of the dark current occurs only at 1.2 V , we selected 1 V as a standard bias to measure incident photon-to-current efficiency (IPCE), photocurrent-time (J_p - t) stability profiles and direct O_2/H_2 evolution rates in the two-electrode configuration. As will be shown later, the I-V characteristic of the solar cell, that we used to construct the self-biased water splitting tandem device, also intersects the I-V characteristic of our photoanode at around 1 V and thus seamlessly substitutes the external bias.

Figure 2 shows IPCE, chopped light I-V characteristics, O_2/H_2 evolution rates accompanied with faradaic efficiencies and J_p - t stability profiles measured under standard conditions (1 sun, 25°C) and under the combination of concentrated light and elevated temperature (3 suns, 50°C). The IPCE characteristics measured at 25°C and 50°C show similar dependence on wavelength with the optical band onsets at 516 nm (2.4 eV) and plateaus in shorter wavelengths that reach 90% and 92%, respectively. The theoretical photocurrent of 6.73 mA cm^{-2} obtained by integrating the product of the IPCE measured at 25°C with the AM1.5G photon flux over all wavelengths is close to the experimental value of 6.72 mA cm^{-2} at the bias of 1 V . Similar calculations for the IPCE measured at 50°C and $3 \times \text{AM1.5G}$ photon flux give the photocurrent value of 20.9 mA cm^{-2} , which is higher than the experimental value of 18.2 mA cm^{-2} implying increased recombination at higher light intensities. Figure 2c,d show the gas production rates of O_2 and H_2 with simultaneously recorded J_p - t profiles. The H_2 and O_2 evolved at stoichiometric ratio with the H_2 generation rates of $102 \mu\text{mol h}^{-1} \text{ cm}^{-2}$ (at 1 sun, 25°C) and $281 \mu\text{mol h}^{-1} \text{ cm}^{-2}$ (at 3 suns, 50°C). The J_p - t curves were used to calculate the theoretical gas production rates and the faradaic efficiencies. The faradaic efficiencies reach 80% within the first 15 minutes and later saturate at $\sim 85\%$, which is a typical value for PEC reactors with a single compartment where oxygen dissolved from the photoanode can undergo a partial back reaction at the Pt counter electrode.

The systematic studies of the photonode performance under different light intensities (0.5–3 suns) and cell temperatures (25 – 50°C) reveal non-linear dependence of the photocurrent on the light flux (see Supplementary Fig. S8). The combined effect of light intensity (I) and temperature on the photocatalytic performance of BiVO_4 has not been studied before. According to Tabata *et al.*²⁶, the hydrogen evolution rate for photocatalytic $\text{K}_4\text{Nb}_6\text{O}_{17}$ nanoparticles is proportional to $I^{0.92}$ at low light intensities (<1 sun) and to $I^{0.52}$ at high light intensities. A similar non-linear response to the light intensity was reported in other studies of photocatalytic water splitting^{31,32} and organic pollutants degradation^{33,34} by TiO_2 . The linear dependence of the photocurrent on the photon flux is valid as long as the photocatalytic reaction at the photoanode/electrolyte junction is faster than recombination rate. As the light intensity increases, the recombination rate becomes dominant causing a half-order dependence on light intensity. Since the sub-linear response represents competition between photocatalytic reaction and recombination rates, the former can be improved by increasing the cell temperature according to the Arrhenius kinetics law. The concept of positive influence of elevated temperature on photocatalytic water splitting was firstly proposed by Licht³⁵ and experimentally reported by Hong *et al.*³⁶ for TiO_2 and by Katakis *et al.*³⁷ for WO_3 . Here we used this approach to improve the photocatalytic reaction kinetics at the BiVO_4 +CoPi/electrolyte interface and extend the linear dependence of the photocurrent on the photon flux to higher light intensities.

The photocurrent (J_p) of the optimized WO_3 -NRs/ BiVO_4 +CoPi photoanode measured under 1 V bias vs a Pt counter electrode shows a typical sub-linear dependence on light intensity at room temperature with $J_p \sim I^m$ and $m = 0.54$ (Supplementary Fig. S8a). This behavior corresponds to the domination of recombination at high light intensities. The intensity exponent m then increases toward unity with

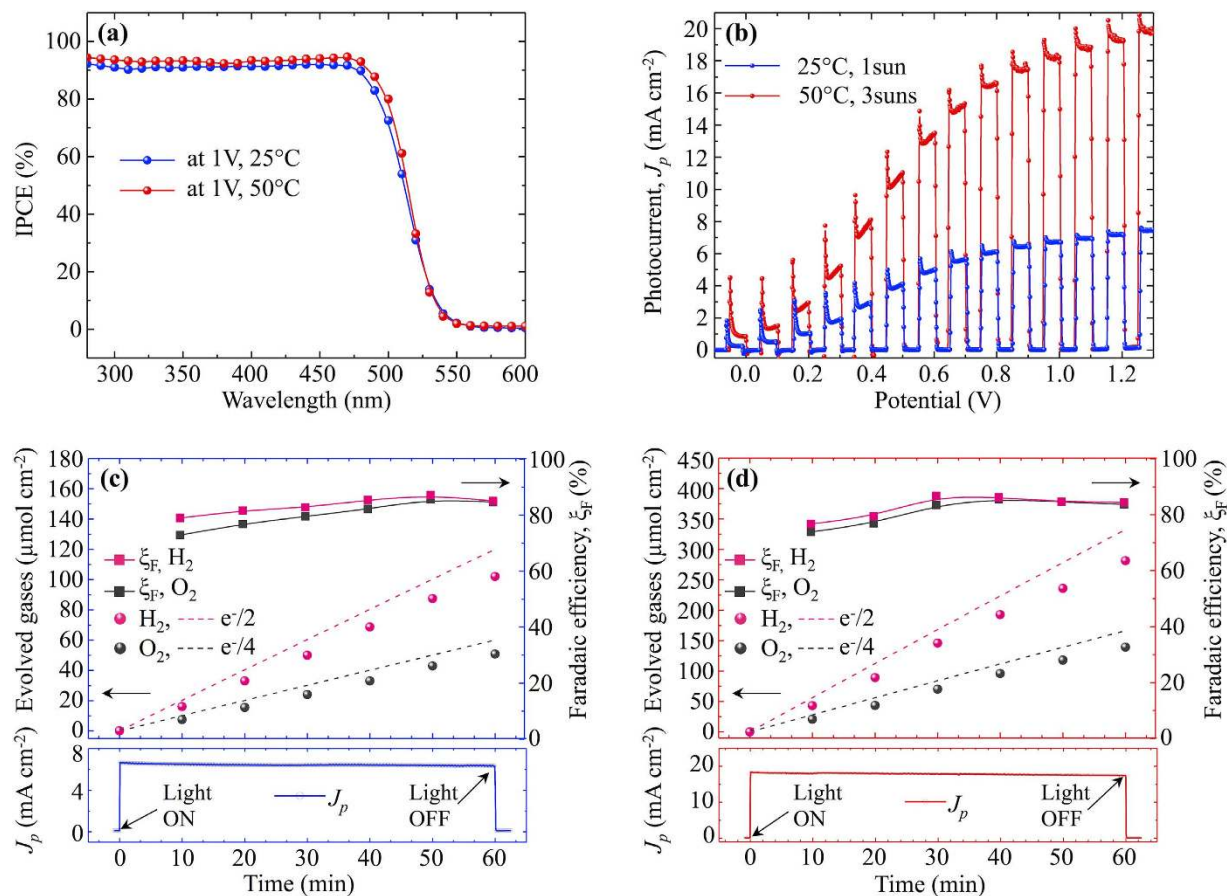


Figure 2. Photoelectrochemical performance of a $\text{WO}_3\text{-NRs/BiVO}_4\text{+CoPi}$ photoanode measured by the two-electrode method under the bias of 1 V. (a) IPCE measured at 25°C (blue) and 50°C (red), (b) I-V characteristics measured under chopped light at 1 sun, 25°C and at 3 suns, 50°C. (c) and (d) gas production rates (circles), faradaic efficiencies (rectangles) and theoretical gas production rates (dashed lines) of O_2 (black) and H_2 (red) for 1 sun, 25°C (c) and for 3 suns, 50°C (d) with simultaneously recorded J_p -t profiles.

increasing temperature and reaches 0.93 at 50°C due to improved reaction kinetics (Supplementary Fig. S8b). It is important to mention that solar thermal collectors with anti-reflecting flat panels can reach temperatures of around 50–60°C even under 1 sun illumination³⁸, while concentrated sunlight can easily heat a water splitting cell to 50–60°C without special measures (Supplementary Fig. S9). The photocurrent of 18.2 mA measured at 3 suns and 50°C corresponds to the quantum efficiency of 81%. As far as we know, this is the first report of efficient water splitting by a $\text{WO}_3\text{-NRs/BiVO}_4$ photoanode under concentrated light.

The water splitting photocurrent can be described as $J_p = J_A \times P_{sep} \times P_{inj}$, where P_{sep} and P_{inj} are separation and injection efficiencies that represent the fractions of holes that reach the photoanode/electrolyte interface and injected into the electrolyte to oxidize water, respectively, while J_A is the rate of photon absorption expressed as a current density. The separation and injection efficiencies characterize bulk and surface recombination processes. Dotan *et al.*³⁹ proposed a method to independently estimate P_{sep} and P_{inj} by measuring J_p in the electrolyte that contains hole scavenger such as H_2O_2 . This method relies on the assumption that the hole scavenger (H_2O_2) removes the injection barrier making $P_{inj} = 1$ without affecting the charge separation. We characterized our photoanodes in the electrolyte containing 0.5 M of H_2O_2 under different light intensities and found no dependence on temperature or significant difference between samples with and without CoPi (see Supplementary Fig. S8c) in the high potential region around 1 V. According to Dotan *et al.*³⁹ the independent estimation of P_{sep} and P_{inj} can be done only in the case of absence of current transients in H_2O_2 containing electrolyte under chopped light. The positive current transients upon turning the light on correspond to the accumulation of holes at the electrode/electrolyte interface. In our case we always observe current transients in the low voltage region (see Supplementary Fig. S14). The transient spikes diminish significantly in the high voltage region and upon temperature increase. This means that independent estimation of P_{sep} and P_{inj} is partially possible only in the high potential region. Supplementary Fig. S8d shows P_{sep} and P_{inj} vs light intensity for two different temperatures 25°C and 50°C. The P_{sep} is almost constant around 90–95% and does not depend

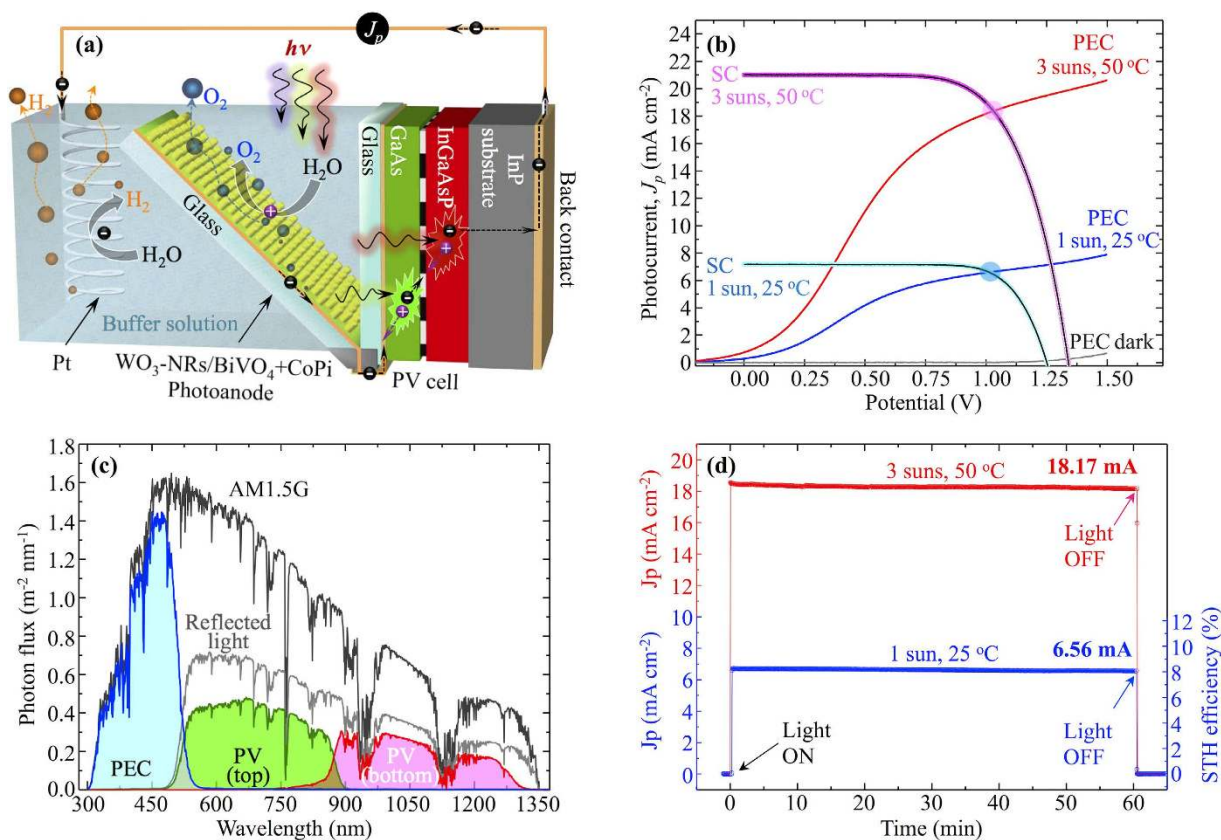


Figure 3. Characterization of PEC-PV tandem device. (a) Schematic illustration of the PEC-PV tandem with the PV cell operating under reflected light from the photoanode. (b) I-V characteristics of the PV cell and the photoanode measured at standard (1 sun, 25°C) and concentrated light (3 suns, 50°C) conditions. (c) Utilization of the incident AM1.5G solar light by the tandem device calculated from the IPCE of the PEC-PV tandem sub-cells and the reflectance spectra of the photoanode. (d) J_p -t profiles measured for the PEC-PV tandem at 1 sun, 25°C (blue) and 3 suns, 50°C (red).

on light intensity and temperature. This is expected behavior for the core-shell ETA structure, where the diffusion length of the photogenerated carriers is much longer than the thickness of the absorber layer. Indeed the diffusion length in BiVO_4 is 80 nm while the thickness of the BiVO_4 layer in our core-shell $\text{WO}_3\text{-NRs/BiVO}_4$ nanostructure is only 25 nm. As a result, P_{sep} is usually close to 1, because electrons can quickly reach the heterojunction interface. In contrast P_{mj} strongly varies with the light intensity and temperature due to competing recombination at surface traps and photocatalytic reaction at the photoanode/electrolyte junction governed by Arrhenius kinetics law.

We demonstrated self-biased water splitting by assembling a tandem device where the $\text{WO}_3\text{-NRs/BiVO}_4\text{+CoPi}$ photoanode is biased by a double-junction mechanically stacked GaAs/AlGaAsP photovoltaic cell. The PV cell was prepared following the previous work of Makita *et al.*⁴⁰ with the top and the bottom cells bonded together by aligned metal nanoparticle arrays. The details on the construction and characterization of the PEC-PV tandem cell can be found in experimental section (also see Supplementary Figures S10 and S11). In order to avoid optical losses associated with inferior transparency of the nanostructured $\text{WO}_3\text{-NRs/BiVO}_4$ photoanode, we located the PV cell parallel to the incident light in such a way that it operated under the light reflected from the photoanode Fig. 3a). The incorporation of the ITO/Pt/ITO stack allowed us to simultaneously maximize reflectance and minimize resistive losses in the photoanode. We would like to emphasize that this configuration can be easily used in a water splitting panel module with segmented light concentrators, such as the one proposed by Turner⁴¹. Figure S12 shows a possible structure of the module that accommodates O_2 and H_2 collecting tranches fitted with the PEC-PV tandem and the Pt counter electrode, respectively, and with hemispherical light concentrators on the top of the module. Other types of optical concentrators that are already developed in the field of low concentration photovoltaics (low-CPV) can also be used to enable non-tracking operation⁴².

Figure 3b shows separately measured I-V characteristics of the PV and the PEC cells at 1 sun (25°C) and 3 suns (50°C) with intersection points at 6.6 mA (at 1.01 V) and 18.3 mA (at 1.02 V), respectively. Although our photoanode is located at 45° with respect to the incident light, its I-V characteristic does

not differ much from the one measured at the normal incident angle. This benefit arises from the long core-shell $\text{WO}_3/\text{BiVO}_4$ nanorods that can capture light equally efficiently from any incident angle in contrast to photoanodes based on flat films. Figure S13 compares I-V characteristics measured at 90° and 45° incident angle for the photoanodes based on core-shell nanorods and flat films. The flat film photoanode shows notable difference in the photocurrent depending on the incident angle, which is mainly attributed to reflective optical losses typical for flat films.

The I-V characteristics of the PV cell were measured under the light reflected from the photoanode. We also measured the I-V characteristics of the PV cell without the photoanode in the tandem assembly to confirm that the PV cell is oriented parallel to the incident light and does not receive additional light from parasitic reflections (see Supplementary Fig. S10c). Indeed, the I-V characteristics in the absence of the photoanode were very close to the ones measured at dark conditions. Figure 3d shows the J_p - t profiles measured for the tandem cell at 1 sun, (25°C) and at 3 suns (50°C) with stabilized photocurrents of 6.56 mA and 18.17 mA, respectively. The photocurrent of 6.56 mA corresponds to the theoretical STH efficiency of 8.1%, which is 1.65 times higher than the previous record of 4.92% reported for $\text{BiVO}_4:\text{W},\text{Mo}/$ double-junction a-Si tandem. The photocurrent of 18.17 mA at 3 suns corresponds to the STH efficiency of 7.5%. Figure 3c shows utilization of the incident AM1.5G solar light by the tandem device that is calculated from the IPCE spectra of the PEC-PV tandem subcells and the reflectance spectra of the photoanode. The IPCE spectra of the PV cell and the PEC-PV tandem are shown in Supplementary Figures S10a and S10b, respectively. The reflectance of the photoanode was not exceeding 60% in the wavelength region $>516\text{ nm}$ due to highly nanostructured ETA configuration. This is the reason why we had to use a highly efficient GaAs/AlGaAsP PV cell in order to generate the matching photocurrent under the weak reflected light. Although, operations under concentrated light can compensate the high cost of the PV cell to some degree, we acknowledge that a more economically viable solution has to be used in the future. Previously, PV assisted photoelectrolysis based on a GaAs/GaInP₂ double-junction solar cell⁴³ or CIGS mini-modules⁴⁴ demonstrated STH efficiencies of 16% and 10.5%, respectively. However, in both cases a highly acidic 3 M H_2SO_4 electrolyte was used to achieve efficient photoelectrolysis, which raises concerns about stability of the cells. Also, PV cells with rather high open-circuit potential $V_{oc} > 1.6\text{ V}$ are required to provide sufficient overpotential for the photoelectrolysis. In contrast, our photoanode efficiently works in a neutral electrolyte at $\text{pH} = 7$ and requires a much lower bias of around 1 V, that is in the range of recently developed inexpensive perovskite solar cells with V_{oc} of 1.15 V⁴⁵. Furthermore, high optical losses originating from low reflectance of the photoanode at $\lambda > 516\text{ nm}$ can be avoided by using a spectral splitting dichroic mirror that provides dedicated portions of the solar spectrum to the PV cell and to the photoanode separately. Therefore, we believe that an economically viable PEC-PV tandem based on a $\text{WO}_3\text{-NRs}/\text{BiVO}_4$ photoanode with STH of around 8% can be realized in the near future.

In conclusion, we utilized an extremely thin absorber concept to fabricate a highly efficient water splitting photoanode based on a $\text{WO}_3\text{-NRs}/\text{BiVO}_4+\text{CoPi}$ core-shell nanostructured heterojunction with the record photocurrent of 6.72 mA measured at 1.23 V_{RHE} under the AM1.5 simulated solar light. To the extent of our knowledge, this is the highest photocurrent reported up to the date among all photoanode materials. Also, we firstly demonstrated an efficient performance of a $\text{WO}_3\text{-NRs}/\text{BiVO}_4$ -based photoanode under concentrated light. We found that an enhanced recombination in BiVO_4 , that leads to sub-linear dependence of the photocurrent on the photon flux, can be compensated by elevating operation temperature of the cell, which significantly improves photocatalytic reaction kinetics at the $\text{BiVO}_4+\text{CoPi}/$ electrolyte interface. As a result, we were able to extend the near linear dependence of the photocurrent on the photon flux to higher light intensities and demonstrate a stable photocurrent of 18.2 mA measured at 3 suns and 50°C under the equivalent bias of 1 V. Finally, we constructed a tandem device based on a $\text{WO}_3\text{-NRs}/\text{BiVO}_4+\text{CoPi}$ photoanode and a GaAs/InGaAsP solar cell operating under reflected light from the photoanode with a stable water splitting photocurrent of 6.56 mA corresponding to the STH efficiency of 8.1%.

Methods

Fabrication of $\text{WO}_3\text{-NRs}/\text{BiVO}_4+\text{CoPi}$ heterojunction photoanodes. Depositions of a ITO/Pt/ITO (150 nm/50 nm/150 nm) stack film and 2.5 μm long $\text{WO}_3\text{-NRs}$ were performed in a multi-magnetron glancing angle deposition (GLAD) system with a 3D rotation stage that allows positioning of the substrate over each magnetron at a desired distance and normal or glancing angle without breaking the vacuum. The formation of uniform WO_3 nanorods instead of a compact thin film was achieved by deposition at a glancing angle, where the shadowing effect⁴⁶ prevents deposition of incident atoms behind spontaneously formed islands (see Fig. 1a). As a result, the morphology of the growing film breaks to columnar while a continuous substrate rotation directs formation of vertically standing and separated nanorods. The as-grown amorphous $\text{WO}_3\text{-NRs}$ were converted to a crystalline monoclinic phase by annealing in air at 575°C for 4.5 hours. The BiVO_4 conformal layer was deposited over the $\text{WO}_3\text{-NRs}$ by a modified electrodeposition method proposed by Seabold *et al.*⁴⁷ from the electrolyte prepared by dissolution of 10 mM $\text{Bi}(\text{NO}_3)_3$ in 35 mM VOSO_4 (adjusted to $\text{pH} = 0.5$ by HNO_3) and then adjusted to $\text{pH} = 4.7$ with a 2 M sodium acetate solution and a few drops of HNO_3 . The electrodeposition was conducted in a two electrode configuration at 55°C under the constant potential of 0.21 V vs a Pt counter electrode. The photoanodes were then annealed in air at 500°C for 2 hours to convert the amorphous BiVO_4 layer to a crystalline monoclinic phase. The CoPi OER co-catalyst was deposited by the photo-assisted

electro-deposition (PED) method following the recipe published by Li *et al.*^{3,6} from the solution of 0.15 M cobalt nitrate in 0.1 M potassium phosphate buffer at constant photocurrent of $\sim 10 \mu\text{A cm}^{-2}$ under 1 sun AM1.5G illumination during 500 s. We also prepared photoanode based on flat film $\text{WO}_3/\text{BiVO}_4$ heterojunction with 900 nm thick compact WO_3 layer and 60 nm thick BiVO_4 layer by using the same fabrication procedure, but without the GLAD regime.

Characterization methods. The photoelectrochemical (PEC) characterizations of the photoanodes were conducted according to the standard PEC characterization protocol⁷ in potassium phosphate buffer solution (pH = 7) by a standard three-electrode method with Ag/AgCl reference and Pt counter electrodes, and by a two electrode method with the bias applied vs a Pt counter electrode. The simulated AM1.5G solar light was adjusted by using an NREL calibrated photodetector. The evolution rates of oxygen and hydrogen were directly measured in an airtight PEC cell connected to a gas micro-chromatograph. The WO_3 -NRs/ BiVO_4 core-shell nanostructures were characterized by X-Ray Diffraction (XRD), Scanning Electron Microscopy (SEM), Energy Dispersive X-ray Spectroscopy (EDS) and Scanning Probe Microscopy (SPM).

Construction of a PEC-PV tandem device. The PV cell consisted of two mechanically stacked GaAs and AlGaAsP solar cells. The p-n junction layers of GaAs ($E_g = 1.42 \text{ eV}$) and $\text{In}_{0.775}\text{Ga}_{0.225}\text{As}_{0.489}\text{P}_{0.511}$ ($E_g = 1.0 \text{ eV}$) were fabricated on GaAs and InP substrates, respectively, by solid source MBE (ss-MBE). Then the GaAs epitaxial layer was separated from the substrate by the epitaxial lift-off (ELO) technique and connected to the AlGaAsP bottom cell through aligned Pd nanoparticle arrays as shown in Fig. S10. The structure was finalized by fabrication of the top AuGe/Ni/Au metal grid and bottom Ti/Au contacts. For more details on the growth of the GaAs and InGaAsP p-n junction layers by ss-MBE, and the transfer of the GaAs layers by ELO and interconnection of the layers by self-assembled Pd nanoparticle arrays, refer to previous works of Makita *et al.*^{40,48}, Sugaya *et al.*^{49,50} and Mizuno *et al.*⁵¹ The solar cell was encapsulated between two thin glass plates with a UV-cured epoxy seal. The PEC-PV tandem was assembled by using a V-shape support where the PEC and the PV cells were located at 45° and parallel to the incident light, respectively. The size of the solar cell was $4 \times 4 \text{ mm}^2$. The widths of the photoanode and the PV cell were 4 mm while the length of the photoanode was equal to the width multiplied by $\sqrt{2}$, i.e. 5.65 mm. Since the photoanode was located at 45° to the incident light, the illuminated area of the tandem device was equal to $4 \times 4 \text{ mm}^2$. In that configuration the PV cell operated only under the light reflected from the photoanode. The I-V characteristics of the solar cell measured under normal illumination and under the light reflected from the photoanode are shown in Fig. S10c and confirm that the PV cell in the PEC-PV tandem was indeed oriented parallel to the incident light and did not receive additional light from parasitic reflections.

References

- Park, Y., McDonald, K. J. & Choi, K. S. Progress in bismuth vanadate photoanodes for use in solar water oxidation. *Chem. Soc. Rev.* **42**, 2321–2337 (2013).
- Abdi, F. F. & van de Krol, R. Nature and light dependence of bulk recombination in CoPi-catalyzed BiVO_4 photoanodes. *J. Phys. Chem. C* **116**, 9398–9404 (2012).
- Abdi, F. F., Savenije, T. J., May, M. M., Dam, B. & van de Krol, R. The origin of slow carrier transport in BiVO_4 thin film photoanodes: a time-resolved microwave conductivity study. *J. Phys. Chem. Lett.* **4**, 2752–2757 (2013).
- Sayama, K. *et al.* Photoelectrochemical decomposition of water into H_2 and O_2 on porous BiVO_4 thin-film electrodes under visible light and significant effect of Ag ion treatment. *J. Phys. Chem. B* **110**, 11352–11360 (2006).
- Chatchai, P., Murakami, Y., Kishioka, S., Nosaka, A. & Nosaka, Y. FTO/ SnO_2 / BiVO_4 composite photoelectrode for water oxidation under visible light irradiation. *Electrochem. Solid-State Lett.* **11**, H160–H163 (2008).
- Berglund, S. P., Flaherty, D. W., Hahn, N. T., Bard, A. J. & Mullins, C. B. Photoelectrochemical oxidation of water using nanostructured BiVO_4 films. *J. Phys. Chem. C* **115**, 3794–3802 (2011).
- Dall'Antonia, L. H. *et al.* Electrosynthesis of bismuth vanadate photoelectrodes. *Electrochem. Solid-State Lett.* **13**, D29–D32 (2010).
- Li, M., Zhao, L. & Guo, L. Preparation and photoelectrochemical study of BiVO_4 thin films deposited by ultrasonic spray pyrolysis. *Int. J. Hydrogen Energy* **35**, 7127–7133 (2010).
- Long, M., Cai, W. & Kisch, H. Visible light induced photoelectrochemical properties of n- BiVO_4 and n- $\text{BiVO}_4/\text{p-Co}_3\text{O}_4$. *J. Phys. Chem. C* **112**, 548–554 (2008).
- Luo, W. *et al.* Solar hydrogen generation from seawater with a modified BiVO_4 photoanode. *Energy Environ. Sci.* **4**, 4046–4051 (2011).
- Kanan, M. W. & Nocera, D. G. *In situ* formation of an oxygen-evolving catalyst in neutral water containing phosphate and Co^{2+} . *Science* **321**, 1072–1075 (2008).
- Ye, H., Park, H. S. & Bard, A. J. Screening of electrocatalysts for photoelectrochemical water oxidation on W-doped BiVO_4 photocatalysts by scanning electrochemical microscopy. *J. Phys. Chem. C* **115**, 12464–12470 (2011).
- Zhong, D. K., Choi, S. & Gamelin, D. R. Near-complete suppression of surface recombination in solar photoelectrolysis by “CoPi” catalyst-modified W: BiVO_4 . *J. Am. Chem. Soc.* **133**, 18370–18377 (2011).
- Pilli, S. K. *et al.* Cobalt-phosphate (CoPi) catalyst modified Mo-doped BiVO_4 photoelectrodes for solar water oxidation. *Energy Environ. Sci.* **4**, 5028–5034 (2011).
- Kim, T. W. & Choi, K.-S. Nanoporous BiVO_4 photoanodes with dual-layer oxygen evolution catalysts for solar water splitting. *Science* **343**, 990–994 (2014).
- Abdi, F. F., Firet, N. & van de Krol, R. Efficient BiVO_4 thin film photoanodes modified with cobalt phosphate catalyst and W-doping. *ChemCatChem* **5**, 490–496 (2013).
- Abdi, F. F. *et al.* Efficient solar water splitting by enhanced charge separation in a bismuth vanadate-silicon tandem photoelectrode. *Nat. Commun.* **4**, 2195 (2013).

18. Su, J., Guo, L., Bao, N. & Grimes, C. A. Nanostructured WO₃/BiVO₄ heterojunction films for efficient photoelectrochemical water splitting. *Nano Lett.* **11**, 1928–1933 (2011).
19. Pilli, S. K. *et al.* Efficient photoelectrochemical water oxidation over cobalt-phosphate (CoPi) catalyst modified BiVO₄/1D-WO₃ heterojunction electrodes. *Phys. Chem. Chem. Phys.* **15**, 14723–14728 (2013).
20. Rao, P. M. *et al.* Simultaneously efficient light absorption and charge separation in WO₃/BiVO₄ core/shell nanowire photoanode for photoelectrochemical water oxidation. *Nano Lett.* **14**, 1099–1105 (2014).
21. Pihosh, Y. *et al.* Nanostructured WO₃/BiVO₄ photoanodes for efficient photoelectrochemical water splitting. *Small*, **10**, 3692–3699 (2014).
22. Shi, X. *et al.* Efficient photoelectrochemical hydrogen production from bismuth vanadate-decorated tungsten trioxide helix nanostructures. *Nat. Commun.* **5**, 4775 (2014).
23. Garnett, E. & Yang, P. Light trapping in silicon nanowire solar cells. *Nano Lett.* **10**, 1082–1087 (2010).
24. Sawada, S. & Danielson, G. Optical indices of refraction of WO₃. *Phys. Rev.* **113**, 1008–1013 (1959).
25. Li, J., Bhalla, A. & Gross, L. Temperature sensitivity of the optical constants of BiVO₄. *Opt. Commun.* **92**, 115–118 (1992).
26. Tabata, S., Ohnishi, H., Yagasaki, E., Ippommatsu, M. & Domen, K. Light-intensity dependence in photocatalytic decomposition of water over K₄Nb₆O₁₇ catalyst. *Catal. Lett.* **28**, 417–422 (1994).
27. Brilliet, J. *et al.* Highly efficient water splitting by a dual-absorber tandem cell. *Nature Photonics* **6**, 824–828 (2012).
28. Miller, E. L., Marsen, B., Cole, B. & Lum, M. Low-temperature reactively sputtered tungsten oxide films for solar-powered water splitting applications. *Electrochem. Solid-State Lett.* **9**, G248–G250 (2006).
29. da Silva, M. *et al.* Deposition and characterization of BiVO₄ thin films and evaluation as photoanodes for methylene blue degradation. *J. Solid State Electrochem.* **16**, 3267–3274 (2012).
30. Chen, Z. *et al.* Accelerating materials development for photoelectrochemical hydrogen production: Standards for methods, definitions, and reporting protocols. *J. Mater. Res.* **25**, 3–16 (2011).
31. Ruan, C., Paulose, M., Varghese, O. K. & Grimes, C. A. Enhanced photoelectrochemical-response in highly ordered TiO₂ nanotube-arrays anodized in boric acid containing electrolyte. *Sol. Energy Mater. Sol. Cells* **90**, 1283–1295 (2006).
32. Bell, S., Will, G. & Bell, J. Light intensity effects on photocatalytic water splitting with a titania catalyst. *Int. J. Hydrogen Energy* **38**, 6938–6947 (2013).
33. Nogueira, R. F. & Jardim, W. F. TiO₂ fixed-bed reactor for water decontamination using solar light. *Sol. Energy* **56**, 471–477 (1996).
34. Jiang, D., Zhao, H., Jia, Z., Cao, J. & John, R. Photoelectrochemical behaviour of methanol oxidation at nanoporous TiO₂ film electrodes. *J. Photochem. Photobiol., A* **144**, 197–204 (2001).
35. Licht, S. Efficient solar generation of hydrogen fuel – a fundamental analysis. *Electrochem. Commun.* **4**, 790–795 (2002).
36. Hong, W. S., Park, J. H. & Han, G. Y. Optimization of conditions for hydrogen production from anodized TiO₂ nanotube-based photoelectrochemical cells. *J. Nanosci. Nanotechnol.* **9**, 7293–7297 (2009).
37. Katakis, D., Mitsopoulou, C. & Vrachnou, E. Photocatalytic splitting of water: increase in conversion and energy storage efficiency. *J. Photochem. Photobiol., A* **81**, 103–106 (1994).
38. Kalogirou, S. A. Solar thermal collectors and applications. *Prog. Energy Combust. Sci.* **30**, 231–295 (2004).
39. Dotan, H., Sivula, K., Grätzel, M., Rothschild, A. & Warren, S. C., Probing the photoelectrochemical properties of hematite (α-Fe₂O₃) electrodes using hydrogen peroxide as a hole scavenger. *Energy Environ. Sci.* **4**, 958–964 (2011).
40. Makita, K. *et al.* Over 20% efficiency mechanically stacked multi-junction solar cells fabricated by advanced bonding using conductive nanoparticle alignments. *MRS Proceedings* **1538**, 167–171 (2013).
41. Turner, J. Oxygen catalysis: the other half of the equation. *Nat. Mater.* **7**, 770–771 (2008).
42. Rudnitsky, A., Zaban, A. & Zalevsky, Z. Passive high ratio sunlight concentration configurations. *J. Europ. Opt. Soc. Rap. Public.* **8**, 13033–7 (2013).
43. Khaselev, O., Bansal, A. & Turner, J. High-efficiency integrated multijunction photovoltaic/electrolysis systems for hydrogen production. *Int. J. Hydrogen Energy* **26**, 127–132 (2001).
44. Jacobsson, T. J., Fjallstrom, V., Sahlberg, M., Edoff, M. & Edvinsson, T. A monolithic device for solar water splitting based on series interconnected thin film absorbers reaching over 10% solar-to-hydrogen efficiency. *Energy Environ. Sci.* **6**, 3676–3683 (2013).
45. Grätzel, M. The light and shade of perovskite solar cells. *Nat. Mater.* **13**, 838–842 (2014).
46. Robbie, K. & Brett, M. Sculptured thin films and glancing angle deposition: growth mechanics and applications. *J. Vac. Sci. Technol., A* **15**, 1460–1465 (1997).
47. Seabold, J. A. & Choi, K. S. Efficient and stable photo-oxidation of water by a bismuth vanadate photoanode coupled with an iron oxyhydroxide oxygen evolution catalyst. *J. Am. Chem. Soc.* **134**, 2186–2192 (2012).
48. Makita, K. *et al.* Highly efficient and reliable mechanically stacked multi-junction solar cells using advanced bonding method with conductive nanoparticle alignments. *40th IEEE PVSC*, Denver USA, 0495–0498 (doi: 10.1109/PVSC.2014.6924968) (2014, June 8–13).
49. Sugaya, T. *et al.* InGaP/GaAs tandem solar cells fabricated using solid-source molecular beam epitaxy. *Jpn. J. Appl. Phys.* **53**, 05FV06–4 (2014).
50. Sugaya, T. *et al.* MBE-grown InGaP/GaAs/InGaAsP triple junction solar cells fabricated by advanced bonding technique. *40th IEEE PVSC*, Denver USA, 0542–0545 (doi: 10.1109/PVSC.2014.6924978) (2014, June 8–13).
51. Mizuno, H., Makita, K. & Matsubara, K. Electrical and optical interconnection for mechanically stacked multi-junction solar cells mediated by metal nanoparticle arrays. *Appl. Phys. Lett.* **101**, 191111–4 (2012).

Acknowledgements

The authors gratefully acknowledge the financial support from the CREST (Core Research for Evolutional Science and Technology) of the Science and Technology Corporation (JST) of Japan and from the New Energy Development Organization (NEDO) of Japan. Also, the authors would like to thank Dr. Hongxuan Guo from NIMS for assistance with SPM measurements and Dr. Takehiko Nagai, Dr. Takashi Koida, Dr. Hitoshi Sai, Dr. Koji Matsubara and Dr. Shigeru Niki from AIST for infrastructural and organizational support.

Author Contributions

Y.P. and I.T. designed the photoanode concept and conceived most experiments on fabrication of WO₃-NRs by GLAD and BiVO₄+CoPi by electrodeposition, materials characterization by SEM, XRD, EDS and PEC performance evaluation. I.T. and Y.P. proposed and realized PEC-PV tandem device, and carried out characterization of PEC and PEC-PV tandem performance under concentrated light and elevated

temperatures. J.U. and S.K. assisted with electrolytes preparation, samples annealing and materials characterization. D.F. supervised and interpreted SPM measurements. K.M., T.S. and T.M. designed and fabricated PV cell for the tandem device. Y.P. and I.T. wrote the manuscript. Y.P., K.M., Y.K., M.T., M.K. and T.K. supervised this project. All authors contributed to manuscript revisions.

Additional Information

Supplementary information accompanies this paper at <http://www.nature.com/srep>

Competing financial interests: The authors declare no competing financial interests.

How to cite this article: Pihosh, Y. *et al.* Photocatalytic generation of hydrogen by core-shell $\text{WO}_3/\text{BiVO}_4$ nanorods with ultimate water splitting efficiency. *Sci. Rep.* **5**, 11141; doi: 10.1038/srep11141 (2015).



This work is licensed under a Creative Commons Attribution 4.0 International License. The images or other third party material in this article are included in the article's Creative Commons license, unless indicated otherwise in the credit line; if the material is not included under the Creative Commons license, users will need to obtain permission from the license holder to reproduce the material. To view a copy of this license, visit <http://creativecommons.org/licenses/by/4.0/>